Bioactive Materials 5 (2020) 667–679

Contents lists available at ScienceDirect

Bioactive Materials

journal homepage: http://www.keaipublishing.com/biomat

Gene-activated dermal equivalents to accelerate healing of diabetic chronic wounds by regulating inflammation and promoting angiogenesis

Dong Lou[a,b], Yu Luo[a], Qian Pang[a], Wei-Qiang Tan[b,**], Lie Ma[a,*]

[a] MOE Key Laboratory of Macromolecular Synthesis and Functionalization, Department of Polymer Science and Engineering, Zhejiang University, Hangzhou, 310027, PR China

[b] Department of Plastic Surgery, Sir Run Run Shaw Hospital, Zhejiang University School of Medicine, Hangzhou, 310016, PR China

ARTICLE INFO

Keywords:
Gene-activated dermal equivalent
Vascular endothelial growth factor
Inflammation
Angiogenesis
Diabetic chronic wounds

ABSTRACT

Diabetic chronic wound, characterized by prolonged inflammation and impaired angiogenesis, has become one of the most serious challenges in clinic and pose a significant healthcare burden worldwide. Although a great variety of wound dressings have been developed, few of encouraged achievements were obtained so far. In this study, the gene-activated strategy was applied to enhance sustained expression of vascular endothelial growth factor (VEGF) and achieve better healing outcomes by regulating inflammation and promoting angiogenesis. The gene-activated bilayer dermal equivalents (Ga-BDEs), which has good biocompatibility, were fabricated by loading the nano-sized complexes of Lipofectamine 2000/plasmid DNA-encoding VEGF into a collagen-chitosan scaffold/silicone membrane bilayer dermal equivalent. The DNA complexes were released in a sustained manner and showed the effective transfection capacities to up-regulate the expression of VEGF in vitro. To overcome cutaneous contraction of rodents and mimic the wound healing mechanisms of the human, a reformative rat model of full-thickness diabetic chronic wound was adopted. Under the treatment of Ga-BDEs, speeding wound healing was observed, which is accompanied by the accelerated infiltration and phenotype shift of macrophages and enhanced angiogenesis in early and late healing phases, respectively. These proved that Ga-BDEs possess the functions of immunomodulation and pro-angiogenesis simultaneously. Subsequently, the better regeneration outcomes, including deposition of oriented collagen and fast reepithelialization, were achieved. All these results indicated that, being different from traditional pro-angiogenic concept, the up-regulated expression of VEGF by Ga-BDEs in a sustained manner shows versatile potentials for promoting the healing of diabetic chronic wounds.

1. Introduction

As one of the most common and serious complications of diabetes mellitus, diabetic foot ulcers (DFU), which are developed in almost 25% diabetic patients, normally result in a chronic wound due to the impairment of healing [[1–3]]. More seriously, under the clinical treatment of traditional wound dressings, 15–20% of DFU will deteriorate and ultimately require amputation [4]. Therefore, it is of significant importance to develop next-generation wound dressing to promote the healing of DFU in clinic.

Being Different from normal cutaneous wound, the pathogenic triad of DFU including neuropathy, ischaemia and inflammation, is frequently occurred [5]. Among them, inflammation, characterized by a low-grade inflammatory state pre-injury and a prolonged inflammatory response post-injury, is detrimental to wound closure and results in a non-healing chronic wound. It means that DFU fails to progress through the orderly phases of healing and is normally detained in a self-perpetuating inflammatory stage [6]. Moreover, because of non-enzymatic glycation of vascular basement membranes of diabetic wound, impaired angiogenesis is also happened and becomes one of the main reasons to inhibit DFU healing [7]. Therefore, in a pathological view, the strategies of modulating inflammation and promoting angiogenesis should be effective and pertinent to accelerate healing of diabetic chronic wounds.

As to angiogenesis, it is of great interest to explore the potential of VEGF family. Many studies have shown that VEGF-A, produced in response to hypoxia, is the most dominant pro-angiogenic factor in normal healing wounds [8,9]. Its expression reaches a peak at 2–3 days post-injury and persists at an elevated level for about one week [10]. However, in contrast to normal mice, the increase of VEGF for

Peer review under responsibility of KeAi Communications Co., Ltd.

* Corresponding author.
** Corresponding author.
E-mail addresses: tanweixxxx@zju.edu.cn (W.-Q. Tan), liema@zju.edu.cn (L. Ma).

https://doi.org/10.1016/j.bioactmat.2020.04.018
Received 22 February 2020; Received in revised form 17 April 2020; Accepted 24 April 2020

congenitally diabetic db/db mice after wounding is transient and not sustained, and it fleetly plummets to barely detectable levels as granulation tissue forms [11]. Therefore, according to the positive results of VEGF application in many pervious researches [12], a proper method to increase VEGF expression should be feasible to promote healing of diabetic chronic wounds.

As a biological marker of self-perpetuating inflammatory stage of diabetic chronic wounds [13], the infiltration of excessive neutrophils, which is responsible for cleaning off active growth factors, degrading excess extracellular matrix and enlarging additional tissue destruction, is always observed. Recent evidences suggest that neutrophil depletion accelerates diabetic wound closure [14,15] and shuts down the inflammatory phase of healing [16]. Considering that neutrophils are eventually engulfed by macrophages, the increasing uptake of apoptotic neutrophils by macrophages would allow diabetic wound to enter into the inflammatory phases [17]. A number of findings verify that neutrophils could directly release growth factors, such as VEGF [18,19] and promote their own removal by monocytes and macrophages [20]. Besides the angiogenesis effect, VEGF is also reported to increases vascular permeability [21] and mediate chemotaxis of monocytes or macrophages via VEGF receptor flt-1 [[22–24]]. Correspondingly, VEGFR-1 blockade disrupts peri-implantation decidual macrophage recruitment and angiogenesis [25]. Considering all information above, it intensely hints that, in early phase, physiological VEGF may exhibit the immunoregulatory functions via facilitating the recruitment of monocytes and macrophages. Therefore, being different from traditional pro-angiogenic concept, the mechanisms of VEGF on accelerating wound healing maybe versatile, including immunoregulation in early phase and pro-angiogenesis in later phase. Therefore, up-regulating expression of VEGF in a sustained manner should be a promising strategy to promote inflammation control and tissue repair of chronic wounds.

Without specific pertinence with pathogenic mechanism of DFU, the alone use of traditional skin equivalents, being in forms of films, sponges, hydrogels and decellularized dermis, gives few of encouraged results so far. Recently, biomaterials with the properties of pro-angiogenesis [26] or anti-inflammation [27] have been applied to improve diabetic wound healing. As discovered in clinic trial results, single dose application of VEGF to wounds alone has limited success due to its short half-life [12]. Repeated topical delivery of VEGF165 promoted rapid reepithelialization and enhanced angiogenesis of diabetic wounds [12]. To overcome the disadvantages of short half-life of VEGF and inconvenience of repeated delivery, delivering VEGF by gene-activated strategy should be promising. It has been reported that the collagen/chitosan scaffolds loaded with plasmid DNA encoding VEGF165 promoted blood vessel formation and faster resorption of the scaffolds [28,29]. Nowadays, most biomaterials therapeutics that focus on single positive pathogenic aspect of diabetic wound healing, such as angiogenesis or anti-inflammation, might have little or no effect on any other. By the gene-activated skin equivalents, the sustained VEGF expression may not only be feasible to improve angiogenesis, but also to regulate inflammation responses to prove its versatile capacity and enhance regeneration outcomes.

Considering its biocompatibility and pro-regeneration effect [28,29], bilayer dermal equivalents (BDEs), consisting of a collagen-chitosan porous scaffold and a silicone membrane, were applied in this study. It was further combined with the lipofectamine 2000/pDNA-VEGF complexes to obtain a gene-activated BDE (Ga-BDEs). After the establishment of type II diabetic rat model, a novel reformative full-thickness diabetic chronic wound was created to prevent skin contraction and mimic humans major healing mechanisms of re-epithelialization and granulation tissue formation. The abilities of inflammatory modulation, angiogenesis and tissue repair of Ga-BDEs were assessed.

2. Experimental

2.1. Materials

Lipofectamine 2000 was purchased from Invitrogen Corporation (Carlsbad, CA). Plasmid DNA encoding enhanced green fluorescence protein (pDNA-eGFP) was a gift from Dr. Jun Li, State Key Laboratory of Diagnosis and Treatment for Infectious Diseases (China). Plasmid DNA encoding human vascular endothelial growth factor-165 (pDNA-VEGF-165) was donated from Dr. Ming Yu, The Fourth Military Medical University (China). The plasmids were amplified in *E. coli* and purified by Axygen Maxiprep Extraction kit (Axygen Biosciences, CA, USA) and stored at −20 °C before use. Chitosan (molecular weight 250 kDa, deacetylation degree 85%) was obtained from Haidebei Co., Ltd (Qingdao, China). Collagen type I was isolated from fresh bovine tendon as described previously [30]. Silicone membrane and the donut-shaped silicone splint were fabricated by a medical grade silicone product from Shanghai Xincheng Co., Ltd (Shanghai, China). Tissue glue used in reformative full-thickness incisional model was produced by Minnesota Mining and Manufacturing Company (3 M, USA). All other reagents were of analytical grade and used as received. Milli Q water was used throughout the experiments.

2.2. Preparation of lipofectamine 2000/pDNA complexes

The plasmid DNA solution of high concentration was diluted with Opti-Minimum Essential Media (MEM) into a concentration of 600 μg/mL. Then, the resulting solution was mixed with Lipofectamine 2000 at a volume ratio of 1:1 by gentle vortex for 3 min. The mixture was further incubated for 20 min at 37 °C to form the stabilized Lipofectamine 2000/pDNA complexes.

2.3. Fabrication of gene-activated bilayer dermal equivalents (Ga-BDEs)

BDEs were prepared according to the procedures described previously [31]. Briefly, collagen and chitosan at a mass ratio of 9:1 were dissolved in 0.5 M acetic acid solution to make a mixture with a total concentration of 0.5% (w/v). Then the collagen-chitosan solution was cross-linked by 0.04% (w/v) glutaraldehyde solution for 4 h at 37 °C. The resulting mixture was injected into a mold, frozen at −20 °C overnight, and then lyophilized for 24 h to obtain collagen-chitosan scaffold. The silicone layer (with a thickness of 0.15 mm) was made from a medical grade silicone membrane (Xincheng Co., Ltd, Shanghai, China). Then, gelatin solution (10% w/v) was homogeneously spread on the silicone layer with an amount of 10 μL/cm^2, which acted as an adhesive to integrate collagen-chitosan scaffold with the silicone layer to form a BDE. After being sterilized by 75% (v/v) ethanol and sufficiently washed with sterilized phosphate buffered saline (PBS, pH 7.4), the extra water of BDEs were sucked quickly by sterilized gauze dressing. Then, 100 μL suspensions of Lipofectamine 2000/pDNA complexes, obtained in section 2.2, were injected into BDE by multi-point injection method, which was followed by 2 h' further incubation at 4 °C to facilitate the adsorption of DNA complexes. Finally, the Ga-BDEs were obtained and the eventual loading amount of DNA was about 3 μg per BDE. Four types of BDEs were prepared in this study, i.e. the blank BDEs, and the BDEs loaded with pDNA-VEGF (BDE + pVEGF), Lipofectamine 2000/pDNA-VEGF complexes (BDE + L/pVEGF), and Lipofectamine 2000/pDNA-eGFP complexes (BDE + L/pGFP), respectively. The pDNA-eGFP was used as a control plasmid to study the potential influence of non-functional DNA.

2.4. Inspection of microstructure characterizations

Ga-BDEs without seeded cells were frozen and lyophilized directly. Ga-BDEs with seeded cells were washed with PBS and then fixed with 4% (w/v) paraformaldehyde at 4 °C for 2 h. After being dehydrated

through water-ethanol gradient solutions and ethanol-isobutanol gradient solution, BEDs were dried by lyophilizing. Then, the BDEs specimens were sputter-coated with a thin gold layer and examined by scanning electronic microscope (SEM, Hitachi, S-3000 N, Japan) with an accelerating voltage of 25 kV.

2.5. Release of DNA complexes from Ga-BDEs

The release of DNA complexes from Ga-BDEs was examined by conducting an in vitro release assay. Ga-BDEs were immersed into 2 mL of sterile PBS at 37 °C. At the scheduled time intervals, 200 μL of the supernatant was collected for analysis, and the same volume of fresh PBS was replenished. The quantity of the released DNA was reacted with Hoechst 33342 (Aladdin, China) and measured by a fluorometer (LS55, PerkinElmer, UK) as described previously [32].

The transfection efficiency of the released DNA complexes was assessed by using the GFP model plasmid and HEK293 cells. After the cells were seeded at a density of 2×10^4 cells per well and cultured for 24 h, DNA complexes released at different time points were added into culture medium with a ratio of 1 μg DNA/10^4 cells. Cells were collected by centrifugation and were re-suspended to analyze the transfection efficiency by a flow cytometry (FACS Calibur, BD Bioscience, USA).

2.6. Cell viability assay

The viability of seeded NIH 3T3 cells (Mouse embryonic fibroblast cells) was analyzed by MTT assay. Briefly, four kinds of BDEs were placed in 24-well plates respectively and 100 μL NIH 3T3 cell suspension, at a density of 5×10^5 cells/mL, was dripped onto the surface of BDEs. After 4 h' cell adhesion, the cell-seeded BDEs were transferred to new plates to exclude cells directly adhered on the plate surface, and further cultured in 500 μL of fresh medium at 37 °C in an atmosphere containing 5% CO_2. The culture medium was changed every 2 d if necessary. At the scheduled time intervals, the culture medium was replaced and supplemented with 60 μL MTT solution (2.5 mg/mL MTT/PBS) for further 4 h incubation. Then the medium was removed, and the scaffolds were transferred to another culture well. 300 μL dimethyl sulfoxide (DMSO) were added to dissolve the formazan crystals. 200 μL supernatant were pipetted and placed in a 96-well plate to test the optical density using a Microplate Reader (Bio-Rad, model 680, USA) at a wavelength of 570 nm.

2.7. In vitro VEGF expression

VEGF expression of HUVECs (Human umbilical vein endothelial cells) cultured on the gene-activated scaffolds in vitro was examined by enzyme-linked immunoabsorbance assay (ELISA). At the scheduled time intervals, the scaffolds were washed three times with PBS (pH 7.4) and then homogenized in the lysis buffer (0.1 M Tris-HCl, 2 mM EDTA, 0.1% Triton X-100). The lysate was then centrifuged at 12,000 rpm at 4 °C for 5 min to collect the supernatant. The amount of VEGF was determined by VEGF ELISA Kit (Bo Shi De Biotech Company, Wuhan, China) according to the manual.

2.8. Animal experiments

Animal experiments were performed according to the Guidelines for Animal Care and Use Committee of Zhejiang University. Sprague-Dawley (SD) rats (male, six weeks old) were obtained from Zhejiang Academy of Medical Sciences and maintained under standard light-dark cycle at ambient temperature (23 ± 2 °C) and humidity (55 ± 10%). After fed high-fat-diet (> 10% fat, > 25% sugar, > 2.5% cholesterol) (Research diets, Boaigang Co., Ltd, Beijing, China) for 4 weeks, SD rats were given a single injection of freshly dissolved streptozotocin (STZ, 40 mg/kg, Sigma) in a 0.1 M citrate buffer (pH 4.5) into peritoneum. One week later, the rats with fasting random blood glucose levels greater than 16.7 mmol/L were selected as the type II diabetic rats [33]. The blood glucose fluctuation and wound healing discrepancy between control and diabetic rats were shown in Table S1 and Fig. S1. Briefly, diabetic rats were anesthetized by intraperitoneal injection of 4% (w/w) pentobarbital solution (0.2 mg/100 g) and sterilized with 5% povidone-iodine. Four full-thickness excisional wounds with the diameter of 8 mm were created symmetrically on the mid-dorsum with a biopsy punch. After the implantation of BDEs, a donut-shaped silicone splint (with a thickness of 1 mm) was fixed on each wound by sutures and tissue glue (3 M) to prevent wound contraction. At the scheduled time points of post-surgery, the macroscopic appearances of the wounds were recorded with a digital camera (Meizu, Zhuhai, China). The tissue specimens at each time interval were harvested.

2.9. Wound analysis

The images of the wounds at different time points after surgery were analyzed by Image J software. The re-epithelization is normally regarded as the complete closure of a wound. In this study, to trace the wound closure process, the ratio of the unhealing area (UA, i.e the unepithelization area) to the original wound area was recorded with the healing time. Three parallel wounds at each time point were analyzed to obtain the averaged unhealing ratio.

2.10. Histological examination

The harvested specimens were fixed with 4% paraformaldehyde at 4 °C overnight, and then dehydrated with a graded series of ethanol and embedded by paraffin. The sectioned samples with a thickness of 5 μm were performed with hematoxylin-eosin (H&E) or Masson's trichrome stainings, and then visualized by the optical microscope (IX81, Olympus, Japan).

2.11. Immunohistochemistry and immunofluorescence staining

To investigate the cytological behaviors of macrophages and new-formation of blood vessels, the macrophages recognizing markers F4/80, M2 macrophages phenotype marker CD163 and endothelial cell marker CD31 were detected by immunohistochemistry and immunofluorescence staining. The paraffin sections (5 μm) were deparaffinized and washed three times in PBS (pH 7.4) for 5 min, and then blocked with 5% serum for 30 min. The slides were subsequently exposed to rat anti-F4/80 primary antibody (1:50, Santa Cruz, Texas, USA) and mouse anti-CD31 primary antibody (1:50, Abcam, Cambridge, UK) at 4 °C overnight, respectively. After being rinsed three times with PBS, the slides were incubated with goat anti-rat and anti-mouse secondary antibodies (1:200, Dako, CA, USA) at 37 °C for 30 min, and further developed with 3, 30-diaminobenzidine tetrahydrochloride (DAB) solution and finally counterstained with hematoxylin. Positive staining was indicated by a brown color observed under an optical microscope (IX81, Olympus, Japan).

Immunofluorescence was performed following the procedures described previously [34]. Briefly, the paraffin sections (5 mm) were deparaffinized, washed in PBS, blocked with 5% serum and incubated overnight at 4 °C with rat anti-F4/80 primary antibody (1:50, Santa Cruz, Texas, USA) and rabbit anti-CD163 primary antibody (1:50, Abcam, Cambridge, UK). After rinsed with PBS, the slides were incubated with rhodamine-conjugated goat-anti-rabbit secondary antibody and FITC-conjugated goat-anti-rat secondary antibody (1:50; Dako, CA, USA) for 30 min. After washed three times in PBS, the cell nuclei were stained by Hoechest (Beyotime, Shanghai, China) for 10 min at room temperature. Images were acquired with a fluorescence microscope (IX81, Olympus, Japan).

2.12. Western blotting analysis

Western blotting (WB) analysis was performed to quantify the translation level of macrophages relevant proteins and newly-formed blood vessels relevant proteins. In vivo samples were harvested and frozen in liquid nitrogen until use. The frozen samples were completely homogenized in RIPA lysis buffer (150 mM sodium chloride, 0.5% Triton X-100, 0.5% sodium deoxycholate, 0.1% sodium dodecyl sulfate (SDS), 50 mM Tris, pH 8.0) with protease inhibitors. The lysates were then clarified by centrifugation at 12,000 rpm at 4 °C for 15 min, and separated on SDS-PAGE. After being transferred to a polyvinylidene fluoride (PVDF) membrane (Millipore, MA, USA), the proteins were incubated overnight with antibodies and detected with an ECL (ECL Western Blotting Substrate, Pierce, USA) system following treatment with 5% milk powder in Tris buffered saline (TBS) to prevent non-specific reaction. The specific antibodies used for this experiment were mouse anti-VEGF primary antibody (Abcam, Cambridge, UK), mouse anti-CD31 primary antibody (Abcam, Cambridge, UK) and goat anti-α-SMA primary antibody (Abcam, Cambridge, UK), chicken anti-F4/80 primary antibody (Abcam, Cambridge, UK), rabbit anti-Arginase 1 primary antibody (Abcam, Cambridge, UK), rabbit anti-GAPDH primary antibody (Abcam, Cambridge, UK).

2.13. Statistical analysis

Data were expressed as mean ± standard deviation (SD). Statistical analysis was performed by two-tailed student's t-tests between two groups or by one-way ANOVA between more groups. The significant level was set at $p < 0.05$.

3. Results and discussion

3.1. Gross view and microstructure of Ga-BDEs

As shown in Fig. 1A, Ga-BDE with a diameter of 8 mm was consisted of two layers, i.e. the collagen-chitosan porous scaffold as the upper layer and the silicone membrane as the lower layer. The bilayer microstructure was further presented by SEM images (Fig. 1B). It showed that the pores of the collagen-chitosan scaffold were highly interconnected to form the porous and open-pore structure, which is more suitable for cell infiltration and nutrition exchange. After the incorporation of DNA complex, the scaffold displayed the similar porous structure and had an average pore size of about 101 ± 20 μm, which was slightly smaller than that of the blank scaffold (115 ± 37 μm) (Fig. 1C and D). From the enlarged SEM images, it was observed that many particle-like lipofactamine2000/plasmid complexes with a size of 0.5–1 μm were adhered on the pore walls of Ga-BDE (Fig. 1E and F).

3.2. Release pattern and in vitro transfection efficiency

The profile of the DNA complexes released from Ga-BDE was displayed in Fig. 2A. It showed that the incorporated DNA complexes could be released in a sustained manner for at least 2 weeks. Based on the slope, the release rate got slower as time goes on, and the rate was high during the first few days. 50% of DNA complexes were released at the first 3 days, and more than 80% at day 14 (Fig. 2A). The transfection abilities of the released DNA complexes were assessed by GFP model plasmid qualitatively. It showed that, compared to that of the freshly prepared DNA complexes, the numbers of the GFP-positive HEK 293 cells became fewer and fewer with the increase of the releasing time, indicating the declining transfection abilities along with release time (Fig. 2B–E). The quantitative results by flow cytometry in Fig. 2F showed that the in vitro transfection efficiency of the released DNA complexes decreased from 56.5 to 13.4% accompanied by the gradually declining release rate. It is worth noting that the released DNA complexes still kept the transfection ability even at day 9 (Fig. 2F, E).

3.3. Biocompatibility and in vitro VEGF expression

As one of main cell types participating in wound regeneration, fibroblast is reliable to evaluate the biocompatibility of Ga-BDE, due to its large quantity and ubiquity in different healing phases. Hence, NIH 3T3 cells (Mouse embryonic fibroblast cells) were seeded into Ga-BDE to observe morphology changes under SEM (Fig. 3A). Compared to the un-spread morphology at day 1 (Fig. 3A a, b), NIH 3T3 cells showed the more spreading morphology with radially extended pseudopodium after 3 days' culture (Fig. 3A c, d), and appeared to be a fully-spreading status to get large adherence area at day 6 (Fig. 3A e, f). Moreover, the result of HE staining shows that the surface of scaffolds was full of NIH 3T3 cells, some of which even infiltrated into the scaffold deeply after 6d culture (Fig. 3B). The fluorescent images also presented the growing status of NIH 3T3 cells on Ga-BDEs, showing that the multiplying quantity, the increasing spread area and typical fusiform morphology was appearing along with the culture time (Fig. 3C a-m). Furthermore, the viabilities of the seeded cells were detected by MTT test to assess the cytotoxicity of Ga-BDE quantitatively (Fig. 3D). The viabilities of NIH 3T3 cells in all BDEs increased monotonously with the culture time. Although no significant difference was found between the four groups at day 1 and 3, both BDE + L/pVEGF and BDE + pVEGF showed significantly higher viability than those of blank BDE and BDE + L/pGFP after 6 days' culture.

As natural VEGF-receptor cells, HUVEC cells were chosen to assess Ga-BDE's effect on VEGF expression. Fig. 3E displays the VEGF expressions of HUVECs cultured into different BDEs in vitro. In all four BDEs, the amounts of the expressed VEGF augmented with the culture time. At each interval, the up-regulated VEGF expressions of HUVECs in BDE + L/pVEGF and BDE + pVEGF were significantly higher than those of the other two groups, which should be attributed to the in vitro transfection of VEGF plasmids. Furthermore, due to the protection and effective delivery by Lipofectamine 2000, the VEGF expression levels of BDE + L/pVEGF were always higher than those of BDE + pVEGF and achieved about two-fold the expression levels after 6 days' culture (Fig. 3E).

3.4. Reformative animal model and macroscopic observations of wounds

SD rat, one of the attractive rodents for wound healing study, was chosen as the model animal in this study due to their availability, low cost, and ease of handling. However, for most rodents, the major mechanism of wound closure is contraction, which is quite different from that of human being, involving reepithelialization and granulation tissue formation [35]. Considering these differences and trying to closely parallel with human wound healing process, in this study, we brought in a reformative full-thickness incisional wound model. After creating a full-thickness incisional wound on the dorsum of a diabetic rat, a donut-shaped silicone splint was placed to prevent contraction, fixed by sutures and tissue glue [35] (Fig. 4A and B). Wound healing was evaluated by the ratio of unhealing area (UA) in the schematic illustration of wound model (Fig. 4A). To avoid wound healing deviation of different implantation sites, four BDEs (①BDE + L/pVEGF, ②BDE + pVEGF, ③BDE + L/pGFP, ④Blank BDEs) were randomly implanted. The typical healing processes and results of different groups were presented in macroscopic observations (Fig. 4C–G). Although the UAs of all BDEs decreased along with the healing time, BDE + L/pVEGF always showed the best healing effects. As displayed in the quantitative results of Fig. 4H, the unhealing ratios of BDE + L/pVEGF were lower than 40 and 20% at day 9 and 15, respectively. An almost complete healing (unhealing ratio < 5%) was observed at day 21, being great ahead of all the control groups (Fig. 4 H).

3.5. HE stainings of wound sections

Wounds samples were harvested at day 3, 9, 15 and 21

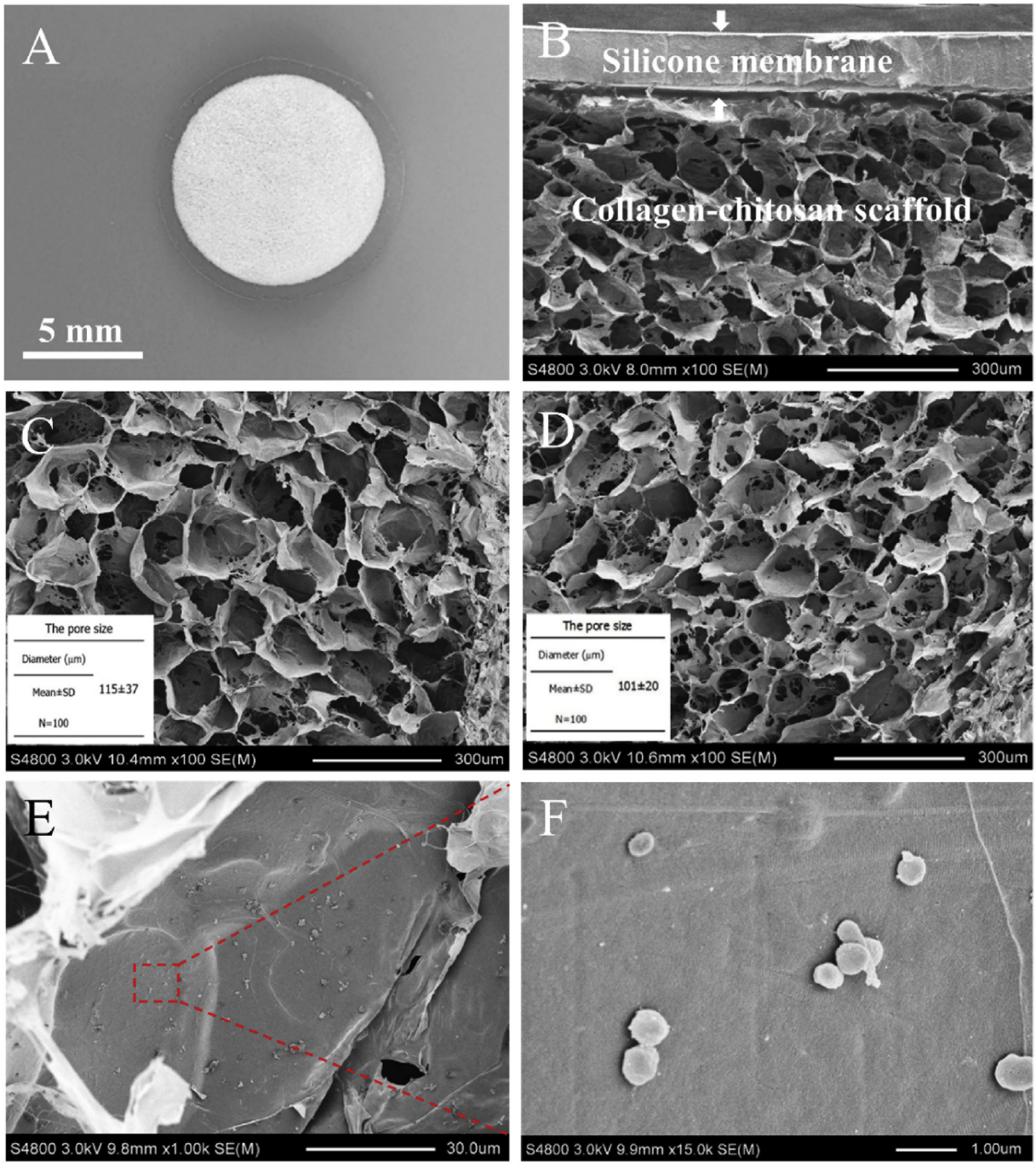

Fig. 1. Gross view and microstructure of Ga-BDEs. (A) Gross view and (B) SEM image of the gene-activated bilayer dermal equivalent (Ga-BDE). (C) is the SEM image of blank collagen/chitosan scaffold. (D) and (E) are the SEM images of lipofactamine 2000/plasmid complex-loaded collagen/chitosan scaffold with different magnifications. (F) is the enlarged view of the red rectangle area of (E) to show the adhered plasmid complexes.

postoperatively for histological analysis to investigate the effects of different BDEs on wound healing (Fig. 5), and the corresponding semi-quantitative results were summarized in Table 1. After 3 days post-operation, it was observed that the newly-formed granulation tissue had begun to grow into the edge of scaffolds for all the groups. For BDE + L/pVEGF, there was no obvious gap between scaffold and host tissue as shown in the other groups (Fig. 5A, E, I, M). Better granulation tissue growth also brought more extracellular matrix (ECM) deposition, appearing as dark and crimson staining, than control groups at day 9 (Fig. 5B, F, J, N; 5b, f, j, n). At day 15, following the indistinction of scaffold edge and epithelial ingrowth, the breadths of the granulation tissues began to decrease in all groups (Fig. 5C, G, K, O). It was particularly evident in BDE + L/pVEGF, indicating that the surrounding normal tissues developed towards the wound center rapidly (Fig. 5C). Accompanying with more oriented ECM deposition and fibroblasts migration at day 21 (Fig. 5d), the area of reepithelialization in BDE + L/pVEGF was extremely larger than those of the other BDEs (Fig. 5D, H, L, P). It should be noted that much more cells with round-nucleus, a typical character of inflammatory cells, were found to been recruited to the injury site of BDE + L/pVEGF in the early healing phase (Fig. 5a). More interestingly, these cells showed a nest-like distribution, being different from the normal distribution of inflammatory cells (Fig. S2).

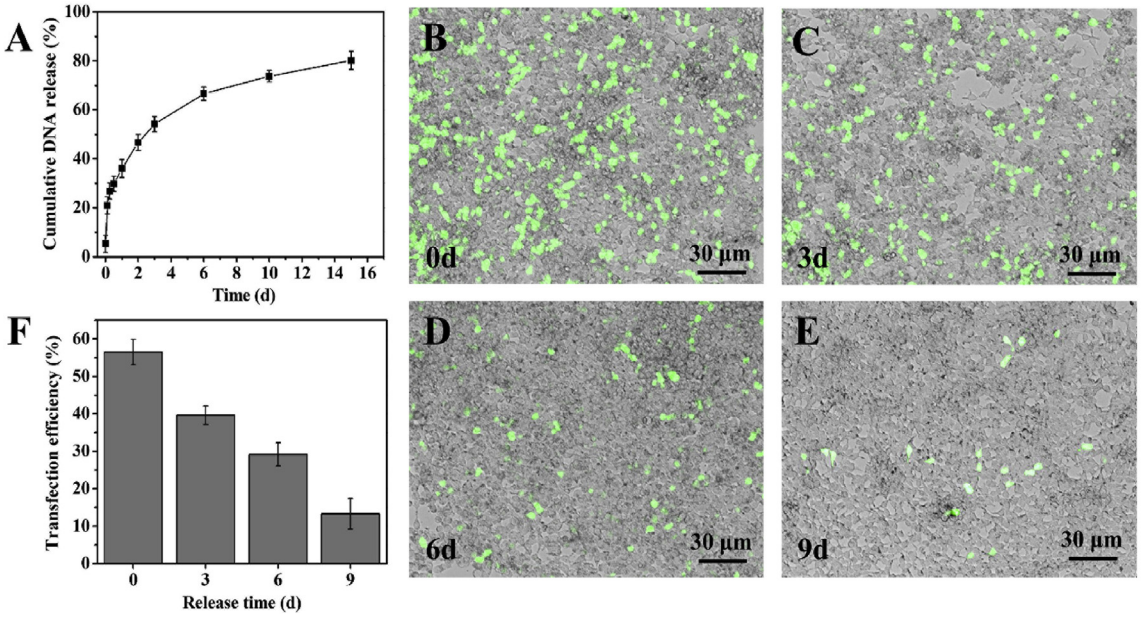

Fig. 2. Release pattern and transfection efficiency of released plasmid complexes. (A) Cumulative release of plasmid complexes from BDEs. (B–E) are the fluorescence and bright-field merged images, showing the HEK293 cells transfected by the lipofactamine 2000/pDNA-eGFP complexes released from BDEs at 0, 3, 6 and 9 d, respectively. (F) The quantitative vitro transfection efficiencies, correspondingly.

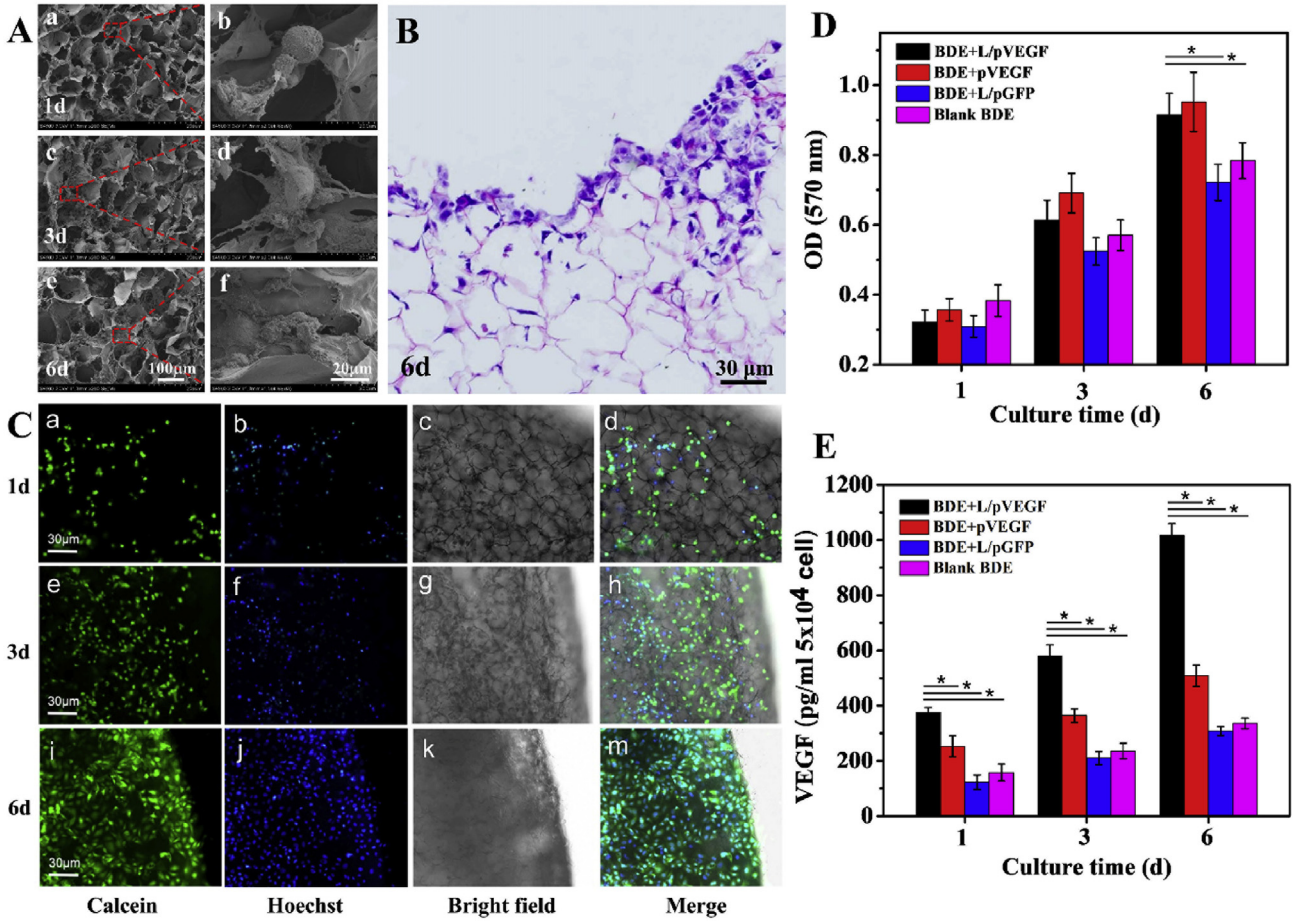

Fig. 3. Biocompatibility evaluation and up-regulated VEGF expression. (A) SEM images of NIH 3T3 cells cultured on Ga-BDEs for 1 (a, b), 3 (c, d) and 6 days (e, f). (b), (d) and (f) are the red rectangle-labeled areas in (a), (c) and (e) with higher magnifications, respectively. (B) H&E staining of the Ga-BDE after seeding NIH 3T3 cells for 6 days. (C) The fluorescence, bright-field, and the corresponding merge images of Ga-BDEs after seeding NIH 3T3 cells for 1 (a–d), 3 (e–h), and 6 days (i–m). NIH 3T3 cells were stained by Calcein and Hoechst, respectively. (D) The viabilities of NIH 3T3 cells being cultured in different BDEs for 1, 3, and 6 days, respectively (n = 3). (E) In vitro VEGF expression of HUVECs after being cultured in different BDEs for 1, 3 and 6 days (n = 3). * denotes statistically significant difference at $p < 0.05$.

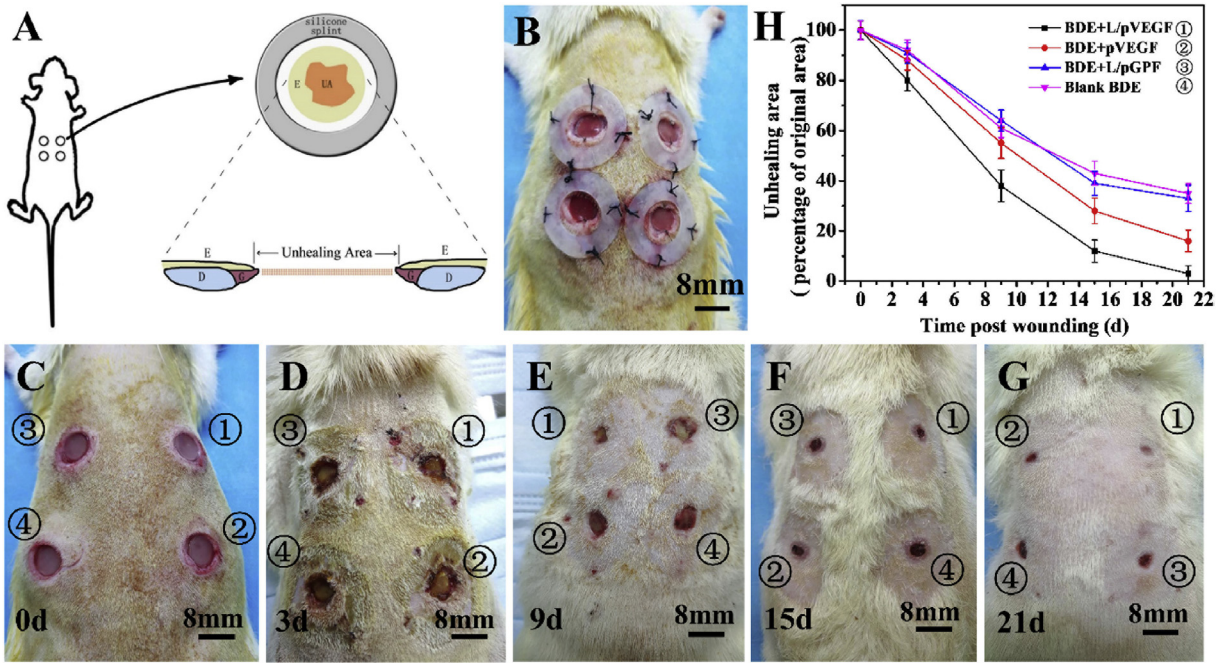

Fig. 4. Reformative animal model and wound healing evaluation. Schematic illustration (A) and representative image (B) of reformative full-thickness incisional model. After creating full-thickness incisional wound, a donut-shaped silicone splint to prevent contraction, was placed and fixed by sutures and tissue glue. The unhealing areas (UA) between bilateral epithelial ingrowth were analyzed using Image J software. E: epithelium, G: granulation tissue, D: dermis. (C–G) are the typical macroscopic observations of the wounds treated by BDEs at different time points. (H) The percentages of UA of the wounds treated by BDEs at different time points. Three wounds at each time point were analyzed to obtain the averaged unhealing ratio.

3.6. Macrophages analysis in early healing phase

Based on our hypothesis that VEGF can regulate inflammation by recruiting monocytes and macrophages to phagocytize excessive neutrophils, it is necessary to figure out the main type and status of inflammatory cell in early healing phase. As anticipated, F4/80 positive macrophages were found to be the main inflammatory cells infiltrated into scaffolds in early healing phase (Fig. 6A a-d). Compared with other control groups, BDE + L/pVEGF had the highest quantity of macrophages (190 ± 11/field) at day 3, which was about triple of the control groups (Fig. 6A a-d, 6C) and meant extensive macrophages infiltration in advance. It was also coincident with the highest F4/80 expression of wound treated by BDE + L/pVEGF (Fig. 6F and G). At day 9, although there was no significant difference on the absolute quantities of macrophages between all groups (Fig. 6C), a declining trend of macrophages quantity was found in BDE + L/pVEGF from day 3–9 (Fig. 6A a, e, C). It was obviously different from the rising trend of other control groups (Fig. 6A b-d, f-h, C), meaning persistent macrophages infiltration and aggregation.

Along with macrophages infiltrating in early healing phase, there were also F4/80 negative and neutrophils-like cells with lobular nucleus (Fig. 6A, the inserts in a-d with magnified details) being recruited to the injury site. Its proportion (< 10%) was the lowest in BDE + L/pVEGF groups at day 3, matching with the highest proportion of macrophages (> 90%) (Fig. 6D). Similar to the variation tendency of quantity in BDE + L/pVEGF, a declining trend of macrophages proportion, from day 3 to day 9, was also found (Fig. 6D), which is opposite to the rising trend of other groups. Moreover, F4/80 negative fibroblasts-like cells with fusiform nucleus were only found in BDE + L/pVEGF group at day 9 (Fig. 6A e, insert with magnified detail). These findings might hint the faster inflammation resolution and the earlier initiation of repair stage in BDE + L/pVEGF.

Hence, F4/80 and CD163 immunofluorescence stainings were conducted to determinate macrophage phenotypes. BDE + L/pVEGF always had the higher ratios of $CD163^+$ macrophages, representing anti-inflammation M2 phenotype, which is about twice as high as the other controls no matter at day 3 or day 9 (Fig. 6B, E). Being not consistent with the declining trend of quantity and proportion, the ratio of $CD163^+$ macrophages rose markedly from day 3–9 in BDE + L/pVEGF (10.8 ± 3.2% to 26.8 ± 5.8%) (Fig. 6B a, e, 6E), indicating the trend of shifting from pro-inflammation to anti-inflammation, which was also proved by western blotting analysis. Accompanying with up-regulated expression of VEGF in early healing phase (Fig. 6F), increasing expressions of F4/80 and Arginase 1 (Fig. 6F, H), a main protein marker for anti-inflammation macrophages phenotype were found in wound treated by BDE + L/pVEGF. In consistence with the ratio change of $CD163^+$ macrophages, BDE + L/pVEGF also obtained the biggest up-regulated trend of Arginase 1 expression (Fig. 6H). Taking into consideration the similar absolute quantities of macrophages between all groups at day 9 (Fig. 6C), the highest relative expression of Arginase 1 in BDE + L/pVEGF group (Fig. 6H) would become more meaningful. Considering all these findings above, it can be speculated that the sustaining up-regulation of VEGF expression by Ga-BDEs promotes more macrophages to be recruited earlier and subsequent shift of macrophage phenotypes from pro-inflammation to anti-inflammation, which is very helpful for the chronic wound to progress through the proper repair stages or, in a sense, break self-perpetuating inflammatory stage.

Interestingly, in our study, under the treatment of Ga-BDEs, the early infiltration of massive macrophages (Fig. 6A a, 6C), normally indicating deteriorative inflammatory response in traditional concept, were observed, with the timely phenotype shift of macrophages and better regeneration outcome subsequently. Although a large of studies put emphasis on accelerating tissue repair by down-regulation of inflammation response, the necessaries of pro-inflammatory molecules to start and intensify the inflammation, have been demonstrated in some cases [[36–39]]. The immune-regulation on chronic wounds should not simply divided into pro-inflammation and anti-inflammation, which must be in a spatiotemporal-matching manner to reconstruct an effective regenerative microenvironment. Usually, excessive neutrophils, a

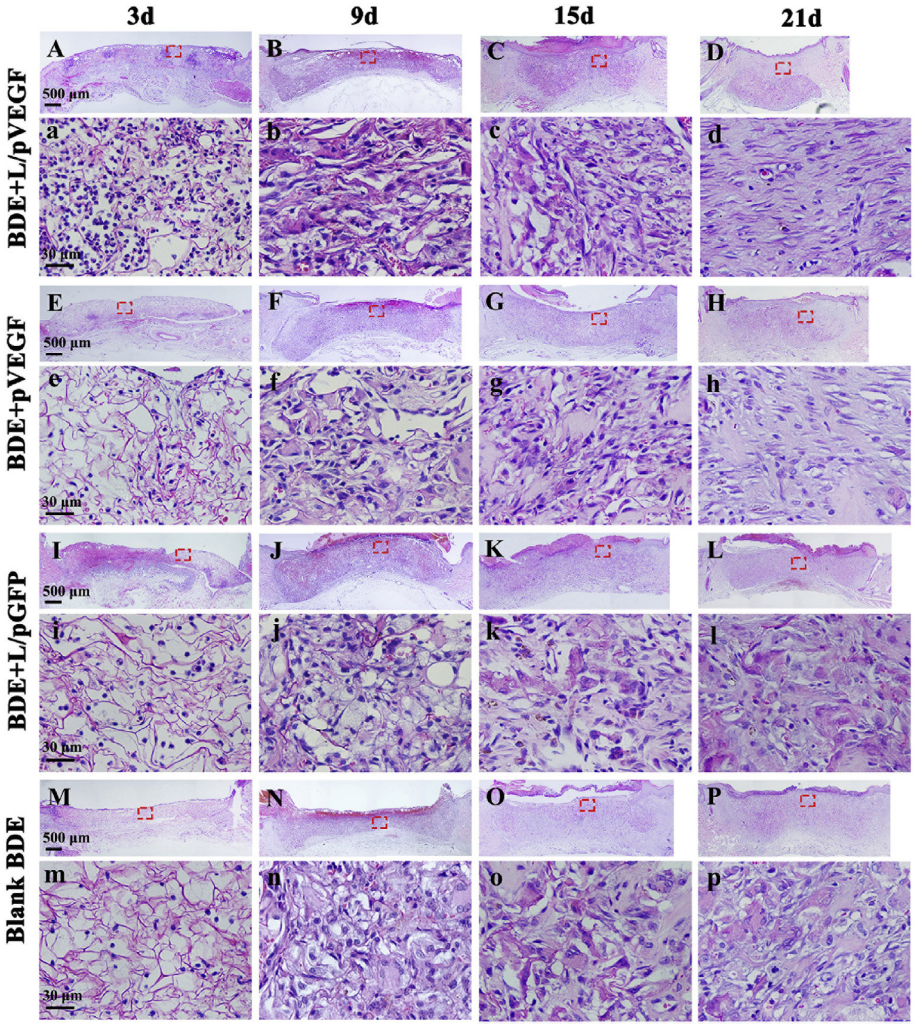

Fig. 5. Histological analysis of wound sections treated by different BDEs. H&E stainings of the whole wounds treated by BDEs loaded with L/pVEGF (A–D), pVEGF (E–H) and L/pGFP (I–L), and blank BDE (M-P) for different days, respectively. (a–d), (e–h), (i–l), and (m–p) are the H&E images with higher magnifications, correspondingly.

Table 1
Tissue responses to the implanted BDEs.

Time	Sample	Granulation tissue	Epithelial ingrowth	Inflammatory cell	Fibroblasts
3d	BDE + L/pVEGF	+	+	+ + +	⊠
	BDE + pVEGF		⊠	+	⊠
	BDE + L/pGFP	⊠	⊠	+	⊠
	Blank BDE	⊠	⊠	+	⊠
9d	BDE + L/pVEGF	+ + +	+ +	+ +	+
	BDE + pVEGF	+ +	+	+ +	
	BDE + L/pGFP	+ +	+	+ +	
	Blank BDE	+ +	+	+ +	
15d	BDE + L/pVEGF	+	+ + +	+	+ +
	BDE + pVEGF	+ +	+	+ +	+
	BDE + L/pGFP	+ +	+	+ +	+
	Blank BDE	+ +	+	+ +	+
21d	BDE + L/pVEGF	⊠	+ + +	⊠	+ + +
	BDE + pVEGF	+	+ +	+	+ +
	BDE + L/pGFP	+ +	+	+ +	+
	Blank BDE	+ +	+	+ +	+

BDEs: collagen-chitosan/silicone membrane bilayer dermal equivalents.
The scores were made from less (+) to abundantly present (+ + +).

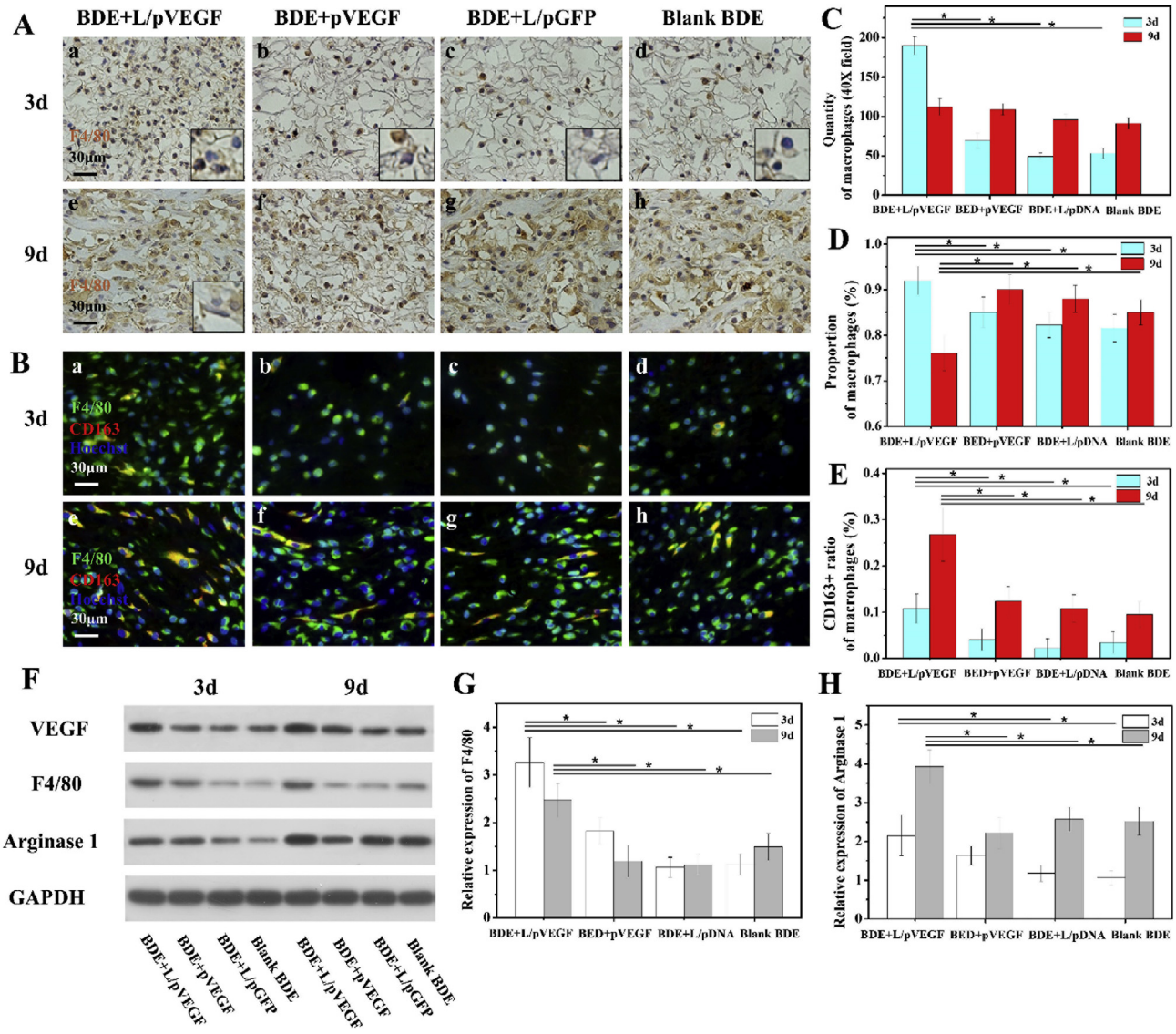

Fig. 6. Macrophages analysis and western blotting test. (A) Immunohistochemical staining of F4/80 of the wounds treated by different BDEs for 3 (A, a-d) and 9 days (A, e-h). The inserts of (A, a-d) are the corresponding detail with higher magnification to show F4/80 negative neutrophils-like cells with lobular nucleus. The insert of (A, e) shows the F4/80 negative fibroblasts-like cells with fusiform nucleus. (B) Triple immunofluorescence of wounds sections treated by different BDEs for 3 (B, a-d) and 9d (B, e-h). Statistics of the quantities (C) and proportions (D) of macrophages, and the proportions of $CD163^+$ macrophages (E) in different groups at day 3 and 9 ($n \geq 3$). (F) Western blotting (WB) of VEGF, F4/80, and Arginase 1 expressions of the wounds treated by different BDEs at different time points. (G, H) Densitometry analyses of the Western blots of F4/80 and Arginase 1 ($n = 3$). * denotes statistically significant difference at $p < 0.05$.

biological marker of self-perpetuating inflammatory stage [13], were removed by monocytes and macrophages [20]. It means that early and sufficient macrophages infiltration may exert anti-inflammation effect by suppressing excessive neutrophil. As one best representation of this mechanism, resolvins are reported to blunt excessive polymorphonuclear neutrophil (PMN) infiltration [40,41] and promote macrophage phagocytosis [40,42]. A number of findings verify that neutrophils could directly release growth factors, such as VEGF-A [18,19] and promote their own removal by macrophages [20]. Hence, early up-regulation of VEGF expression by BDE + L/pVEGF in our study (Fig. 6F), which simulates macrophages recruitment, is likely to enhance neutrophils (Fig. 6A, the inserts) removal to weaken its negative effect, and makes it easier for diabetes chronic wounds to continue the subsequent healing phases.

3.7. Pro-angiogenic effect of Ga-BDEs

To characterize the effects of different BDEs on angiogenesis during wound healing, CD31 immunohistochemistry staining and semi-quantitative analysis of the newly-formed vessels was performed in Fig. 7. At all the time points except for day 21, BDE + L/pVEGF had the highest vessel densities compared to those of the other groups (Fig. 7Q). Unlike the other control groups in which the densities of blood vessels sustainedly increased along with the implantation time from day 3 to day 15, BDE + L/pVEGF showed a peak of blood vessel density (96 ± 8/mm^2) at day 9 uniquely, which was about twice as many as the control groups (Fig. 7Q, E-H black triangle). With the further increase of implantation time, the densities were declined to 78 ± 7 and 54 ± 8/mm^2 at day 15 and 21, respectively. (Fig.7Q). Interestingly, the mature vessels with disc-shaped and nuclei-lack erythrocyte (Fig. 7E, I, M, red arrows) were found in BDE + L/pVEGF from day 9, much earlier than the other control groups, in which no mature vessel was found until day 21 (Fig. 7O, P, red arrows) and even some rounded-nucleus inflammatory cells were still detected (Fig. 7O, P, black arrows). The expression levels of CD31 and α-SMA were analyzed by WB (Fig.7R, S, T). The darkest band of CD31 was found in the group of BDE + L/

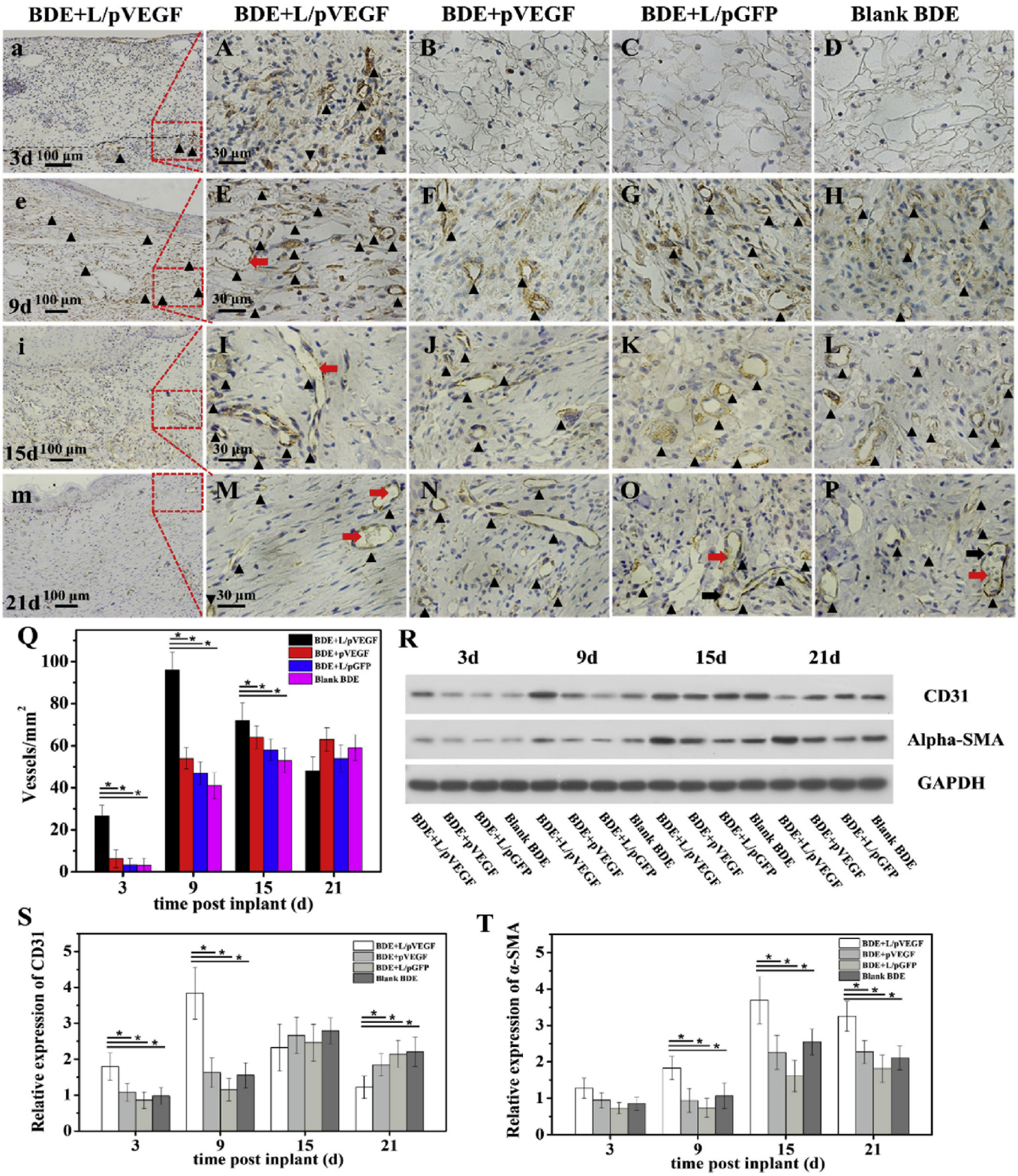

Fig. 7. Pro-angiogenic effect of different BDEs. Immunohistological stainings of CD 31 of the wounds treated by different BDEs for 3 (A–D), 9 (E–H), 15 (I–L), and 21 days (M-P). Red and black arrows show mature vessels with erythrocyte flow and the inflammatory cell being recruited from circulation, respectively. (a, e, i, m) are the overview images with lower magnification of (A, E, I, M) to show the newly-formed blood vessels in L/pVEGF group. Black triangle showed CD 31^+ blood vessels. (Q)The statistic numbers of the newly-formed blood vessels ($CD31^+$ positive stainings) per mm^2 ($n \geq 6$). (R) WB of CD31 and α-SMA expressions of the wounds treated by different BDEs at different time points. (S, T) Densitometry analyses of the Western blots of CD31 and α-SMA ($n = 3$). * denotes statistically significant difference at $p < 0.05$.

pVEGF at day 9, which were consistent with the semi-quantitative results of blood vessel density (Fig. 7Q). It should be noted that BDE + L/pVEGF showed the highest expression of α-SMA, a marker for smooth muscle cells wrapping mature vessels, at day 9,15 and 21 (Fig. 7R, T), which account for the finding of functional vessels with erythrocyte (Fig. 7E, I, M, red arrows) and indicate the effect of BDE + L/pVEGF on accelerating mature of new-formed blood vessels.

In most previous studies, the pro-angiogenesis effect of VEGF was more focused while the inflammation regulating effect in early healing phase was not paid attention to. In the traditional view, inflammatory cells infiltration was accompanyed by granulation formation, angiogenesis and increase of vascular permeability after wound was created. However, not synchronizing with the extensive infiltration of inflammatory cells in early healing phase (Figs. 5a and 6A a), the formation of new blood vessels obviously lagged behind the inflammation process in wound treated by BDE + L/pVEGF. As inflammatory cells have infiltrated the whole wound and BDEs, new blood vessels, stained by CD31 (Fig. 7a black triangle) only took place infrequently on the edge of BDE + L/pVEGF (Fig. 7a black dotted line) at day 3. Distinguished from the decreasing tendency of macrophages from day 3–9 (Fig. 6C and D), the quantity of new-formed blood vessels increased markedly and got a peak at day 9 (Fig. 7Q). Till macrophages decreased and gradually shifted to anti-inflammation phenotype, new-formed blood vessels augmented distribution range and grew into BDEs (Fig. 7e black triangle). Conceivably, the unparalleled even diverging relationship between macrophages infiltration (Fig. 6C and D) and blood vessels neogenesis (Fig. 7 a, e, Q), which is not conforming to the traditional knowledge, suggested the intrinsic versatile characters of VEGF and possible different mechanisms for inflammation regulation and pro-angiogenesis.

Indeed, it's reported that these two functions are mediated via different VEGF trans-membrane receptors, KDR (VEGFR2) and flt1 (VEGFR1) [[22–24]]. Monocytes, in contrast to endothelium expressing VEGFR2 mainly, express only VEGF receptor flt-1. VEGFR-1 null (flt-1 −/−) mutant embryos die because of an overgrowth of vascular endothelial cells [43]. Mice with deletion of VEGFR-1 Tyrosine Kinase (TK) domain (Flt-1 TK−/−) are viable and have normal blood vessel development, but have altered macrophage migration [44]. Therefore, in normal physiological conditions, these two functions mediated via different VEGF receptors may relatively independent and complementary. It explains the limited effect of single dose application of VEGF to wounds in a sense [12]. It suggests that the sustaining up-regulation of VEGF expression in wounds treated by BDE + L/pVEGF can match different spatiotemporal requirements of inflammation regulation and pro-angiogenesis to construct an effective regenerative microenvironment.

3.8. Assessment of tissue remodeling by Masson's staining

Under the regulation effects of VEGF on inflammation regulation and pro-angiogenesis, the better regeneration outcomes should be obtained concomitantly. After the treatment by BDEs for 2–3 weeks, the wounds got access to a remodeling stage. As the representative outcomes, the newly-deposited collagen and keratin were detected by Masson's trichrome, which stains collagen in blue, keratin in red and nuclei in red/brown, respectively. For the group of BDE + L/pVEGF, a continuous keratin-positive layer with a red-strip shape at day 15 and almost intact epidermal layer at day 21 were observed (Fig. 8A, E; black arrows indicate the edges of the keratin-positive layers). Comparably, other groups resulted in the fragmentary and smallish keratin-positive layers, indicating that no complete epidermal layer was formed even at day 21 (Fig. 8B–D, F-H black arrows). With the gradual decay of granulation tissue, the process of tissue remodeling developed towards the wound center. For the wounds treated with BDE + L/pVEGF, BDE was degraded acceleratedly from top to bottom and from outside to inside. Renascent collagen replaced the BDE and deposited much better, more continuous and extensive, in the healing region under renascent epidermal layer (Fig. 8E blue stain). About 4 weeks postoperation, BDE would be completely absorbed in the BDE + L/pVEGF group. While, fewer collagen was observed for the wounds treated with the other three BDEs (Fig. 8F–H blue stain). Beyond augment amount of deposition, the newly-formed collagen became more oriented and regular in BDE + L/pVEGF group (Fig. 8 a, e), reminding accelerated wound healing and better regeneration outcome than other groups (Fig. 8 b-d, f-h).

As a representation of chronic wounds which sustains egregious length of time (usually taken to be more than three months) [45], diabetes chronic wound is traditionally considered as the results of the pathogenic triad including neuropathy, ischaemia and inflammation [5]. Without pertinence to multi pathogenic factors, traditional artificial skin equivalents obtain few encouraged achievement, even combined with single drug delivery strategy. Ideal skin equivalent for diabetes chronic wounds should be easy-operating, effective and covering multiple pathogenic factors. Being different from traditional knowledge of VEGF, a main endothelial mitogen for pro-angiogenesis, its effects on the recruitment and phenotype modulation of macrophages are rarely considered [46,47]. Overcoming the defects of the short half-life of direct-used growth factors and inconvenience of repeated delivery, VEGF gene-activated bilayer dermal equivalents (Ga-BDEs) was proved to be a promising method for diabetes chronic wounds in this study, by its easy-preparation and versatile capacities, including immunoregulation and pro-angiogenesis.

4. Conclusions

By loading L/pVEGF complexes into BDEs, Ga-BDEs for promoting the repair of diabetic chronic wounds were constructed. The loaded DNA complexes were released from the collagen-chitosan porous scaffold in a sustained manner. The in vitro transfection capacities of the released DNA complexes to up-regulate the expression of VEGF persisted till for more than 9 days. Being proved good biocompatibility, the Ga-BDEs were transplanted to the full-thickness diabetic chronic wounds. Accompanying speeding wound healing, the accelerated infiltration and phenotype shift of macrophages and enhanced angiogenesis were observed in early and late healing phases, respectively. Finally, the better regeneration outcomes were achieved in the aspects of oriented collagen deposition and faster reepithelialization. All these results prove that Ga-BDEs can promote the healing of diabetic chronic wounds by modulating immune responses and enhanced angiogenesis, and will show a great potential for chronic wound healing in clinical application in future.

CRediT authorship contribution statement

Dong Lou: Conceptualization, Methodology, Investigation, Data curation, Writing - original draft. **Yu Luo:** Methodology. **Qian Pang:** Methodology, Investigation. **Wei-Qiang Tan:** Conceptualization, Methodology, Supervision. **Lie Ma:** Conceptualization, Supervision, Writing - review & editing, Funding acquisition.

Declaration of competing interest

The authors declare that they have no known competing financial interests or personal relationships that could have appeared to influence the work reported in this paper.

Acknowledgements

The authors acknowledge Dr. Jingyao Chen (the Core Facilities, School of Medicine, Zhejiang University) for his supports on histological analysis. This study is financially supported by the National

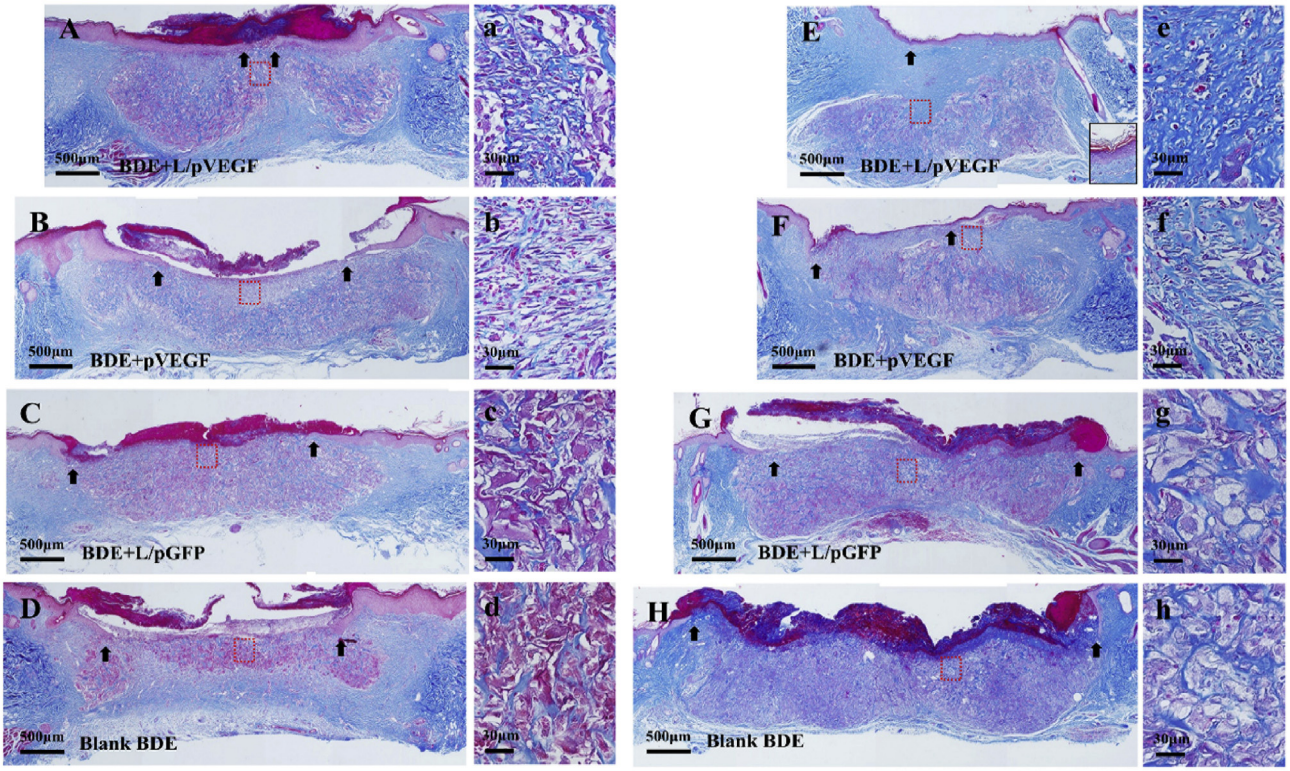

Fig. 8. Assessment of tissue remodeling by Masson's staining. Masson's stainings of the whole wounds treated by different BDEs in later healing phase at 15 d (A–D) and 21 d (E–H). (a–d) and (e–h) are the magnified images of the red rectangle-labeled areas in (A–D) and (E–H), correspondingly. Black arrows show epithelial gaps.

Natural Science Foundation of China (51873184, 81671918) and National Key R&D Program of China (2016YFC1101000).

Appendix A. Supplementary data

Supplementary data to this article can be found online at https://doi.org/10.1016/j.bioactmat.2020.04.018.

References

[1] K. Ogurtsova, R.F.J. Da, Y. Huang, U. Linnenkamp, L. Guariguata, N.H. Cho, D. Cavan, J.E. Shaw, L.E. Makaroff, IDF Diabetes Atlas: global estimates for the prevalence of diabetes for 2015 and 2040, Diabetes Res. Clin. Pract. 128 (2017) 40–50.
[2] D. Baltzis, I. Eleftheriadou, A. Veves, Pathogenesis and treatment of impaired wound healing in diabetes mellitus: new insights, Adv. Ther. 31 (2014) 817–836.
[3] A.J. Boulton, The pathway to foot ulceration in diabetes, Med Clin North Am 97 (2013) 775–790.
[4] G.D. Mulder, L.M. Patt, L. Sanders, J. Rosenstock, M.I. Altman, M.E. Hanley, G.W. Duncan, Enhanced healing of ulcers in patients with diabetes by topical treatment with glycyl-l-histidyl-l-lysine copper, Wound Repair Regen. 2 (1994) 259–269.
[5] V. Falanga, Wound healing and its impairment in the diabetic foot, Lancet 366 (2005) 1736–1743.
[6] R. Zhao, H. Liang, E. Clarke, C. Jackson, M. Xue, Inflammation in chronic wounds, Int. J. Mol. Sci. 17 (2016).
[7] K.A. Kim, Y.J. Shin, J.H. Kim, H. Lee, S.Y. Noh, S.H. Jang, O.N. Bae, Dysfunction of endothelial progenitor cells under diabetic conditions and its underlying mechanisms, Arch Pharm. Res. (Seoul) 35 (2012) 223–234.
[8] N.N. Nissen, P.J. Polverini, A.E. Koch, M.V. Volin, R.L. Gamelli, L.A. DiPietro, Vascular endothelial growth factor mediates angiogenic activity during the proliferative phase of wound healing, Am. J. Pathol. 152 (1998) 1445–1452.
[9] L.F. Brown, K.T. Yeo, B. Berse, T.K. Yeo, D.R. Senger, H.F. Dvorak, L. van de Water, Expression of vascular permeability factor (vascular endothelial growth factor) by epidermal keratinocytes during wound healing, J. Exp. Med. 176 (1992) 1375–1379.
[10] L.F. Brown, K.T. Yeo, B. Berse, T.K. Yeo, D.R. Senger, H.F. Dvorak, L. van de Water, Expression of vascular permeability factor (vascular endothelial growth factor) by epidermal keratinocytes during wound healing, J. Exp. Med. 176 (1992) 1375–1379.
[11] K.G. Peters, C. De Vries, L.T. Williams, Vascular endothelial growth factor receptor expression during embryogenesis and tissue repair suggests a role in endothelial differentiation and blood vessel growth, Proc. Natl. Acad. Sci. U. S. A. 90 (1993) 8915–8919.
[12] R.D. Galiano, O.M. Tepper, C.R. Pelo, K.A. Bhatt, M. Callaghan, N. Bastidas, S. Bunting, H.G. Steinmetz, G.C. Gurtner, Topical vascular endothelial growth factor accelerates diabetic wound healing through increased angiogenesis and by mobilizing and recruiting bone marrow-derived cells, Am. J. Pathol. 164 (2004) 1935–1947.
[13] R.F. Diegelmann, M.C. Evans, Wound healing: an overview of acute, fibrotic and delayed healing, Front. Biosci. 9 (2004) 283–289.
[14] J.V. Dovi, L.K. He, L.A. DiPietro, Accelerated wound closure in neutrophil-depleted mice, J. Leukoc. Biol. 73 (2003) 448–455.
[15] D.M. Simpson, R. Ross, The neutrophilic leukocyte in wound repair a study with antineutrophil serum, J. Clin. Invest. 51 (1972) 2009–2023.
[16] C. Nathan, Neutrophils and immunity: challenges and opportunities, Nat. Rev. Immunol. 6 (2006) 173–182.
[17] A.D. Widgerow, Cellular resolution of inflammation–catabasis, Wound Repair Regen. 20 (2012) 2–7.
[18] E. Kolaczkowska, P. Kubes, Neutrophil recruitment and function in health and inflammation, Nat. Rev. Immunol. 13 (2013) 159–175.
[19] Y. Gong, D.R. Koh, Neutrophils promote inflammatory angiogenesis via release of preformed VEGF in an in vivo corneal model, Cell Tissue Res. 339 (2010) 437–448.
[20] E. Kolaczkowska, P. Kubes, Neutrophil recruitment and function in health and inflammation, Nat. Rev. Immunol. 13 (2013) 159–175.
[21] J.A. Nagy, L. Benjamin, H. Zeng, A.M. Dvorak, H.F. Dvorak, Vascular permeability, vascular hyperpermeability and angiogenesis, Angiogenesis 11 (2008) 109–119.
[22] B. Barleon, S. Sozzani, D. Zhou, H.A. Weich, A. Mantovani, D. Marme, Migration of human monocytes in response to vascular endothelial growth factor (VEGF) is mediated via the VEGF receptor flt-1, Blood 87 (1996) 3336–3343.
[23] M. Clauss, H. Weich, G. Breier, U. Knies, W. Rockl, J. Waltenberger, W. Risau, The vascular endothelial growth factor receptor Flt-1 mediates biological activities. Implications for a functional role of placenta growth factor in monocyte activation and chemotaxis, J. Biol. Chem. 271 (1996) 17629–17634.
[24] C. Sunderkotter, M. Goebeler, K. Schulze-Osthoff, R. Bhardwaj, C. Sorg, Macrophage-derived angiogenesis factors, Pharmacol. Ther. 51 (1991) 195–216.
[25] N.C. Douglas, R.C. Zimmermann, Q.K. Tan, C.S. Sullivan-Pyke, M.V. Sauer, J.K. Kitajewski, C.J. Shawber, VEGFR-1 blockade disrupts peri-implantation decidual angiogenesis and macrophage recruitment, Vasc. Cell 6 (2014) 16.
[26] T.N. Demidova-Rice, J.T. Durham, I.M. Herman, Wound healing angiogenesis: innovations and challenges in acute and chronic wound healing, Adv. Wound Care 1 (2012) 17–22.
[27] L.I. Moura, A.M. Dias, E. Carvalho, H.C. de Sousa, Recent advances on the

development of wound dressings for diabetic foot ulcer treatment–a review, Acta Biomater. 9 (2013) 7093–7114.
[28] R. Guo, S. Xu, L. Ma, A. Huang, C. Gao, Enhanced angiogenesis of gene-activated dermal equivalent for treatment of full thickness incisional wounds in a porcine model, Biomaterials 31 (2010) 7308–7320.
[29] R. Guo, S. Xu, L. Ma, A. Huang, C. Gao, The healing of full-thickness burns treated by using plasmid DNA encoding VEGF-165 activated collagen-chitosan dermal equivalents, Biomaterials 32 (2011) 1019–1031.
[30] L. Ma, C. Gao, Z. Mao, J. Zhou, J. Shen, X. Hu, C. Han, Collagen/chitosan porous scaffolds with improved biostability for skin tissue engineering, Biomaterials 24 (2003) 4833–4841.
[31] L. Ma, Y. Shi, Y. Chen, H. Zhao, C. Gao, C. Han, In vitro and in vivo biological performance of collagen-chitosan/silicone membrane bilayer dermal equivalent, J. Mater. Sci. Mater. Med. 18 (2007) 2185–2191.
[32] Z. Mao, L. Ma, Y. Jiang, M. Yan, C. Gao, J. Shen, N,N,N-Trimethylchitosan chloride as a gene vector: synthesis and application, Macromol. Biosci. 7 (2007) 855–863.
[33] L. Shen, W. Zeng, Y.X. Wu, C.L. Hou, W. Chen, M.C. Yang, L. Li, Y.F. Zhang, C.H. Zhu, Neurotrophin-3 accelerates wound healing in diabetic mice by promoting a paracrine response in mesenchymal stem cells, Cell Transplant. 22 (2013) 1011–1021.
[34] R. Guo, S. Xu, L. Ma, A. Huang, C. Gao, The healing of full-thickness burns treated by using plasmid DNA encoding VEGF-165 activated collagen-chitosan dermal equivalents, Biomaterials 32 (2011) 1019–1031.
[35] R.D. Galiano, J.T. Michaels, M. Dobryansky, J.P. Levine, G.C. Gurtner, Quantitative and reproducible murine model of excisional wound healing, Wound Repair Regen. 12 (2004) 485–492.
[36] M. Kucia, K. Jankowski, R. Reca, M. Wysoczynski, L. Bandura, D.J. Allendorf, J. Zhang, J. Ratajczak, M.Z. Ratajczak, CXCR4-SDF-1 signalling, locomotion, chemotaxis and adhesion, J. Mol. Histol. 35 (2004) 233–245.
[37] T.T. Lau, D.A. Wang, Stromal cell-derived factor-1 (SDF-1): homing factor for engineered regenerative medicine, Expet Opin. Biol. Ther. 11 (2011) 189–197.
[38] C.N. Serhan, N. Chiang, T.E. Van Dyke, Resolving inflammation: dual anti-inflammatory and pro-resolution lipid mediators, Nat. Rev. Immunol. 8 (2008) 349–361.
[39] M.J. Zhang, M. Spite, Resolvins: anti-inflammatory and proresolving mediators derived from omega-3 polyunsaturated fatty acids, Annu. Rev. Nutr. 32 (2012) 203–227.
[40] N. Chiang, G. Fredman, F. Backhed, S.F. Oh, T. Vickery, B.A. Schmidt, C.N. Serhan, Infection regulates pro-resolving mediators that lower antibiotic requirements, Nature 484 (2012) 524–528.
[41] M. Clauss, M. Gerlach, H. Gerlach, J. Brett, F. Wang, P.C. Familletti, Y.C. Pan, J.V. Olander, D.T. Connolly, D. Stern, Vascular permeability factor: a tumor-derived polypeptide that induces endothelial cell and monocyte procoagulant activity, and promotes monocyte migration, J. Exp. Med. 172 (1990) 1535–1545.
[42] G.H. Fong, J. Rossant, M. Gertsenstein, M.L. Breitman, Role of the Flt-1 receptor tyrosine kinase in regulating the assembly of vascular endothelium, Nature 376 (1995) 66–70.
[43] S. Hiratsuka, O. Minowa, J. Kuno, T. Noda, M. Shibuya, Flt-1 lacking the tyrosine kinase domain is sufficient for normal development and angiogenesis in mice, Proc. Natl. Acad. Sci. U. S. A. 95 (1998) 9349–9354.
[44] K.C. Wheeler, M.K. Jena, B.S. Pradhan, N. Nayak, S. Das, C. Hsu, D.S. Wheeler, K. Chen, N.R. Nayak, VEGF may contribute to macrophage recruitment and M2 polarization in the decidua, PloS One 13 (2018).
[45] R. Nunan, K.G. Harding, P. Martin, Clinical challenges of chronic wounds: searching for an optimal animal model to recapitulate their complexity, Dis. Model Mech. 7 (2014) 1205–1213.
[46] C.N. Serhan, N. Chiang, T.E. Van Dyke, Resolving inflammation: dual anti-inflammatory and pro-resolution lipid mediators, Nat. Rev. Immunol. 8 (2008) 349–361.
[47] C.N. Serhan, S.D. Brain, C.D. Buckley, D.W. Gilroy, C. Haslett, L.A. O'Neill, M. Perretti, A.G. Rossi, J.L. Wallace, Resolution of inflammation: state of the art, definitions and terms, Faseb. J. 21 (2007) 325–332.